Scalar wave falloff in asymptotically anti–de Sitter backgrounds

J. S. F. Chan
Department of Applied Mathematics, University of Waterloo, Waterloo, Ontario, Canada N2L 3G1

R. B. Mann
Department of Applied Mathematics, University of Waterloo, Waterloo, Ontario, Canada N2L 3G1
and Department of Physics, University of Waterloo, Waterloo, Ontario, Canada N2L 3G1
(Received 13 December 1996)

Conformally invariant scalar waves in black hole spacetimes which are asymptotically anti–de Sitter spacetimes are investigated. We consider both the $(2+1)$-dimensional black hole and $(3+1)$-dimensional Schwarzschild–anti-de Sitter spacetime as backgrounds. Analytical and numerical methods show that the waves decay exponentially in the $(2+1)$-dimensional black hole background. However, the falloff pattern of the conformal scalar waves in the Schwarzschild–anti-de Sitter background is generally neither exponential nor an inverse power rate, although the approximate falloff of the maximal peak is weakly exponential. We discuss the implications of these results for mass inflation. [S0556-2821(97)02312-6]

PACS number(s): 04.30.Nk, 04.20.Ha, 04.25.Dm, 04.70.−s

I. INTRODUCTION

It is well known that the maximally extended Reissner-Nordström spacetime can be imagined as a collection of different asymptotically flat universes connected by different charged black holes [1]. Except for the Schwarzschild solution, all the special solutions of the more general Kerr-Newman class of spacetimes can have two horizons, the inner and outer horizons. Nevertheless, gravitational theorists find that these dual-horizon black holes are unphysical because causality can be violated inside the hole [2]. Moreover, any radiation (either electromagnetic or gravitational in nature) that goes into this kind of black hole will be indefinitely blueshifted at the inner (or Cauchy) horizon [1]. This effect has caused some to expect that this null hypersurface acts like a barricade to other universes in maximally extended spacetime.

This infinite blueshift phenomenon at the Cauchy horizon was first discussed by Penrose in the late 1960s [3]. At that time, people believed that any small energy perturbation on these dual-horizon black holes would destroy the Cauchy horizon because the perturbation is indefinitely magnified there, causing an infinite spacetime curvature at the horizon. Thus the null hypersurface would become a spacelike curvature singularity and the gateway to other universes is sealed. Both numerical and analytic approaches [4,5] suggest that this null hypersurface is perturbatively unstable. However, although singularities are found at the Cauchy horizon, they are not spacetime curvature singularities at all. By taking the diverging stress-energy tensor into account, Hiscock showed that the perturbation only turns the horizon into a so-called *whimper singularity*: All curvature scalars are finite but a freely falling observer crossing the horizon measures an infinite energy density [6]. This kind of singularity is too mild to seal off the passage to other universes, and so resolution of the issue would necessitate a study that did not rely on perturbation theory.

Poisson and Israel made a breakthrough in this problem by showing that the Cauchy horizon can turn into a scalar spacetime curvature singularity [7]. Unlike Hiscock, who considered a Reissner-Nordström black hole irradiated by a flux of incoming radiation, Poisson and Israel imposed both incoming and outgoing fluxes of radiation on a Reissner-Nordström background. The outgoing flux, even if negligibly small in quantity, makes the inner mass function of the black hole inflate without bound at the Cauchy horizon. More precisely, the inner mass of the black hole diverges at a rate of $\exp(\kappa v)/v^p$ near the Cauchy horizon. The factor $1/v^p$ comes from the decay rate of the scattered radiation tail [7–9], where $p>0$ and $v\to\infty$ at the Cauchy horizon. Regardless of the values of p and the surface gravity $\kappa>0$, the mass parameter always grows, although the exponential rate is attenuated by the decaying effect of the radiation tail. This phenomenon is called *mass inflation* and is expected to seal the inner horizon because the diverging mass parameter induces a scalar curvature singularity at the horizon. This result implies that it is inappropriate to maximally extend any dual-horizon black holes beyond the Cauchy horizon because spacetime is unstable against energy perturbations there. It is generally believed that such perturbations (in the form of gravitational radiation) always exist in more realistic black holes which do not have perfect spherical or axial symmetry. These are scattered around the black hole, forming incoming and outgoing fluxes, but they will eventually decay away as a tail of late time radiation [9]. In this way, mass inflation is expected to prevent violation of causality.

In addition to the Reissner-Nordström black hole, the mass inflation phenomenon has been found to take place in other black hole configurations [10–16]. These configurations are in $1+1$, $2+1$, and $3+1$ dimensions as well as in asymptotically nonflat spacetimes. All of these calculations assumed the inverse power-law decay for late time radiation as an ansatz to obtain the inflating mass function near the Cauchy horizon. Since the mass parameter is attenuated by the decaying effect of the radiation tail, it is important to understand the behavior of the radiative tail in a spacetime

other than Reissner-Nordström class. Mellor and Moss have shown that the radiation from perturbations in a de Sitter background exponentially decreases [17]. Strictly speaking this result has nothing to do with late time falloff because the global geometry extends beyond the cosmological horizon. However, it indicates that the radiative falloff behavior is sensitive to the presence of the cosmological constant. More recent work by Ching *et al.* [18] demonstrated that under certain circumstances the tail can be something other than the simple inverse power law.

In this paper we will study radiative falloff in spacetimes that are not asymptotically flat. We find that the inverse power law [9] is not universally true and that in some asymptotically anti–de Sitter spacetimes the late time tail decays exponentially. The asymptotically anti–de Sitter backgrounds we will study are the $(2+1)$-dimensional black hole [19] and Schwarzschild–anti-de Sitter spacetime.

The outline of our paper is as follows. In Sec. II we review the structure of the $(D+1)$-dimensional scalar wave equation in spherically symmetric spacetimes that are not necessarily asymptotically flat and discuss our numerical approach towards solving it. In Sec. III we verify that our numerical approach correctly reproduces the power-law falloff in asymptotically flat spacetimes, and we cross-check this analytically. In the next two sections we study the falloff behavior in the $(2+1)$-dimensional [or three-dimensional (3D)] black hole background and in $(3+1)$-dimensional Schwarzschild–anti-de Sitter spacetime. Concluding remarks and an appendix round out our work.

II. WAVE EQUATION IN $D+1$ DIMENSIONS

We shall study scalar waves in different dimensions, since wave equations for higher-spin fields are of a qualitatively similar structure [20]. The (conformally coupled) scalar wave equation in $D+1$ dimensions is

$$\nabla^2\Psi=\xi R\Psi, \tag{1}$$

where ξ is an arbitrary constant. If $\xi=(D-1)/(4D)$, this equation is conformally invariant. We simplify the problem by considering only static, spherically symmetric $(D+1)$-dimensional spacetimes with metric

$$ds^2=-N(r)dt^2+\frac{dr^2}{N(r)}+r^2d\Omega_{D-1}^2, \tag{2}$$

where $N(r)$ is the lapse function and $d\Omega_{D-1}^2$ is the metric of a $(D-1)$-dimensional unit sphere. We assume

$$\Psi=r^{(1-D)/2}\psi(t,r)Y_l^D. \tag{3}$$

The functions Y_l^D are the D-dimensional spherical harmonics which satisfy the equation

$$\hat{L}^2[Y_l^D]=-l(l+D-2)Y_l^D. \tag{4}$$

The product $-l(l+D-2)$ is the eigenvalue of the operator $\hat{L}^2$ which is the angular derivative operator. It is straightforward to show that Eq. (1) gives

$$-\partial_{tt}\psi(t,r)+N(r)\partial_r[N(r)\partial_r\psi(t,r)]-N(r)V_e(r)\psi(t,r)=0. \tag{5}$$

The function $V_e(r)$ is defined as

$$V_e(r)\equiv\xi R+\frac{D-1}{2r}\frac{d}{dr}N(r)+\frac{(D-1)(D-3)}{4r^2}[N(r)-1]+\frac{(2l+D-3)(2l+D-1)}{4r^2}. \tag{6}$$

One can rewrite the wave equation (5) as

$$-\partial_{tt}\psi(t,r)+N(r)\mathcal{L}[\psi(t,r)]=0, \tag{7}$$

with the help of a spatial differential operator

$$\mathcal{L}\equiv\partial_r[N(r)\partial_r]-V_e(r). \tag{8}$$

Alternatively, if we introduce

$$x\equiv\int\frac{dr}{N(r)}, \tag{9}$$

then Eq. (5) can be written as

$$\partial_{tt}\psi(t,r(x))-\partial_{xx}\psi(t,r(x))+V(r(x))\psi(t,r(x))=0 \tag{10}$$

or as

$$\partial_{uv}\psi(u,v)=-\tfrac{1}{4}N(r(u,v))V_e(r(u,v))\psi(u,v) \tag{11}$$

using null coordinates $u=t-x$ and $v=t+x$. The function $V(r)$ [defined as $V(r)\equiv N(r)V_e(r)$] plays the role of a potential barrier which is induced from the background spacetime geometry. Although the potential when written in terms of the tortoise coordinate x can be very complicated, Eq. (10) has the familiar form of a potential scattering problem.

Equation (10) can be integrated numerically in a straightforward fashion by using the finite difference method. First of all the D'Alembert operator $\partial_{tt}-\partial_{xx}$ can be discretized as

$$\frac{\psi(t-\Delta t,x)-2\psi(t,x)+\psi(t+\Delta t,x)}{\Delta t^2}-\frac{\psi(t,x-\Delta x)-2\psi(t,x)+\psi(t,x+\Delta x)}{\Delta x^2}+O(\Delta t^2)+O(\Delta x^2) \tag{12}$$

using Taylor's theorem. In order to formulate a well-posed Cauchy problem we need to include the initial conditions, which for simplicity we choose to be

$$\psi(t=0,x)=0 \quad \text{and} \quad \partial_t\psi(t=0,x)=u(x). \tag{13}$$

Because the field ψ is initially zero, its subsequent evolution is solely the result of the initial impulse of the field $\partial_t\psi$. Discretizing the second condition in Eqs. (13) yields

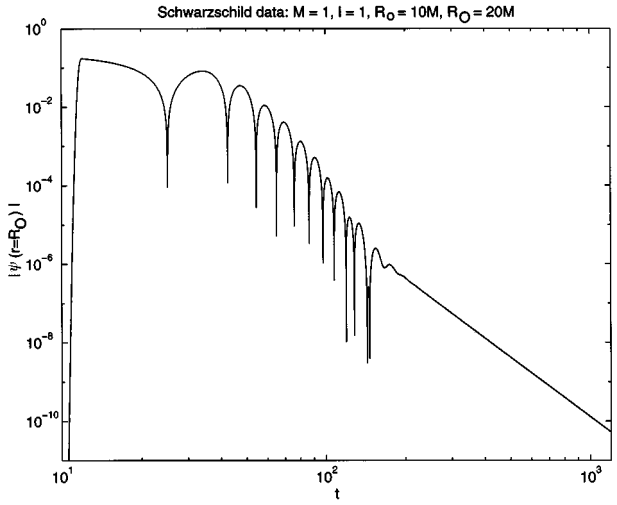

FIG. 1. The decay of a scalar wave in a Schwarzschild background. Prior to $t=200$ the decay is accompanied by a ''ringing'' of the quasinormal modes, after which the falloff rate is that of an inverse power law.

$$\frac{\psi(\Delta t,x)-\psi(-\Delta t,x)}{2\Delta t}=u(x)+O(\Delta t^2), \tag{14}$$

where we employ a Gaussian distribution with finite support for $u(x)$. We further define

$$\psi(m\Delta t,n\Delta x)\equiv\psi_{m,n}, \tag{15}$$

$$V(n\Delta x)\equiv V_n, \tag{16}$$

$$u(n\Delta x)\equiv u_n, \tag{17}$$

where the mesh size has to satisfy the condition $\Delta x>\Delta t$ so that the numerical rate of propagation of data is greater than its analytical counterpart. The discretization of the Cauchy problem above then implies

$$\psi_{-1,n}=-\Delta t u_n, \tag{18}$$

$$\psi_{0,n}=0, \tag{19}$$

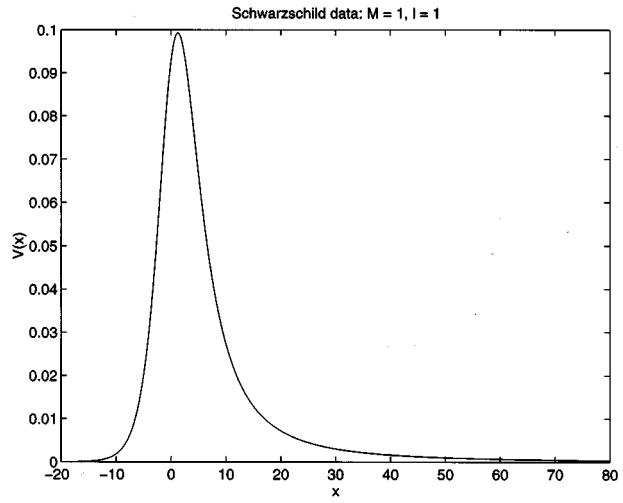

FIG. 2. Potential barrier for the Schwarzschild background.

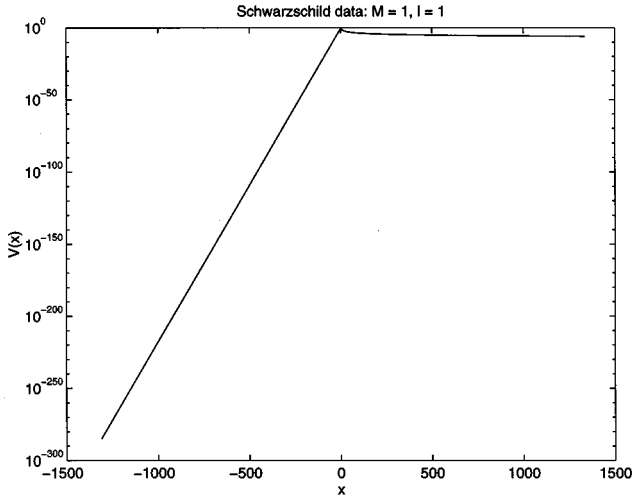

FIG. 3. Exponential decrease on the left side of the barrier in $V(x)$.

$$\psi_{m+1,n}=\left[2-2\frac{\Delta t^2}{\Delta x^2}-\Delta t^2 V_n\right]\psi_{m,n}-\psi_{m-1,n}+\frac{\Delta t^2}{\Delta x^2}[\psi_{m,n-1}+\psi_{m,n+1}]. \tag{20}$$

As a result, we can follow the evolution of the field ψ starting from the initial data given at time $t=0$.

In the case where the black hole geometry is asymptotically flat, the tortoise coordinate x goes from negative infinity to positive infinity. Therefore our Cauchy problem is similar to the infinite string problem in which the initial data propagate towards left and right indefinitely. The initial data no longer enjoy this privilege when the background is an asymptotically anti–de Sitter background because the tortoise coordinate goes from minus infinity to zero only. In other words, the right-propagating data cannot travel in this direction forever. Analogous to the semi-infinite vibrating string problem, boundary conditions at spatial infinity (i.e.,

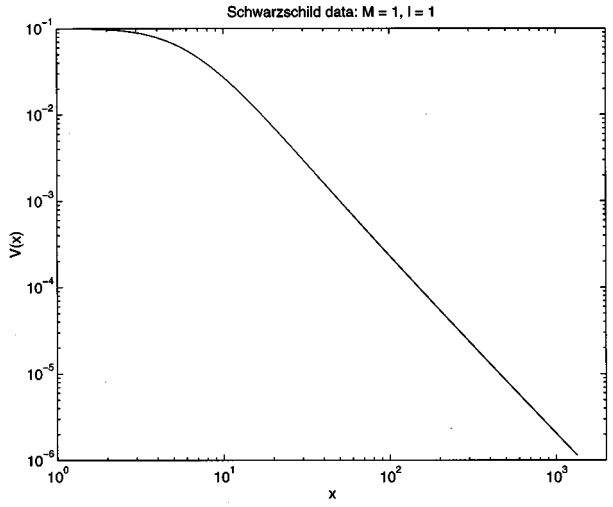

FIG. 4. Inverse power decrease on the right side of the barrier of $V(x)$.

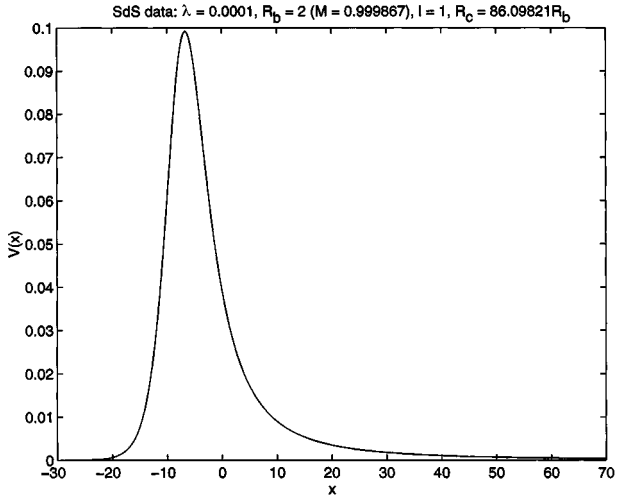

FIG. 5. Potential barrier for the Schwarzschild–de Sitter background.

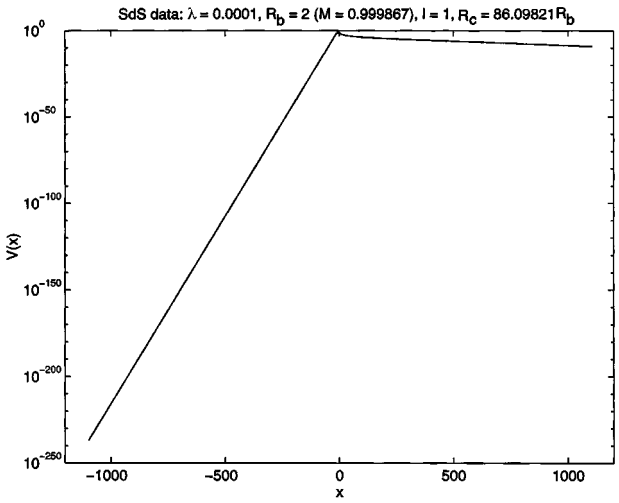

FIG. 6. Exponential decreasing nature on the left side of $V(x)$ in the SdS background.

$x=0$) are needed in the asymptotically anti–de Sitter background in order to formulate the problem appropriately. Two types of boundary conditions that are widely used in anti–de Sitter backgrounds are the Dirichlet and Neumann conditions [21]. In our case, the former reads

$$\psi(t,x=0)=0 \quad \text{and} \quad \partial_x\psi(t,x=0)=1, \tag{21}$$

while the latter is simply

$$\psi(t,x=0)=1 \quad \text{and} \quad \partial_x\psi(t,x=0)=0. \tag{22}$$

We shall consider employing both of these boundary conditions at spatial infinity for our numerical computations whenever the background geometry is an asymptotically anti–de Sitter background.

III. ASYMPTOTICALLY FLAT BACKGROUNDS

In this section we will review the behavior of radiative falloff in asymptotically flat background spacetimes [9]. We will present the results of the numerical calculation first.

Figure 1 shows a sample inverse power decay of a scalar wave in the Schwarzschild background spacetime of mass M. We solve the wave equation (10) numerically using the scheme discussed in the previous section. The compact initial Gaussian impulse is centered at a distance $r=10M$ (or $x=12.76M$) and for simplicity we choose the $l=1$ spherical harmonic. Figure 1 shows how the magnitude of the scalar field ψ at a distance $r=20M$ (i.e., $x=24.40M$) evolves. Using linear regression, we find that the slope of the straight line on the graph is -5.026, in agreement with the analytic prediction of an inverse power-law falloff with exponent $2l+3$ [9].

Figures 2–4 show the same potential barrier $V(x)$ that is responsible for this falloff behavior. Figure 3 shows an exponential decrease of the left side of the potential function; this is a result of the fact that the event horizon is located at $x=-\infty$. On the other hand, the power-law decrease on the right side of $V(x)$ shown in Fig. 4 is a direct consequence of the use of an asymptotically flat background. If we compare Figs. 2–4 with Figs. 5–7, which represent the potential function in Schwarzschild–de Sitter (SdS) spacetime, we find that the right side of $V(x)$ has different decaying behavior even though the overall appearance of $V(x)$ on the linear graph is very similar. It is this difference that distinguishes the falloff behavior in the two backgrounds.

Now let us consider a scalar wave in an asymptotically flat $(D+1)$-dimensional background. For the remainder of this section we will restrict our attention to the case where the number of spatial dimensions D is odd. The motivation for this may be traced back to Huygen's principle, which implies that in even spatial dimensions the scalar wave obeying the equation $\nabla^2\Psi=0$ always develops a tail, regardless of whether or not the asymptotically flat background is sourceless. Consequently identification of the tail part of the wave that is due to solely to backscattering becomes quite problematic when D is even.

Inspired by the work of Ching *et al.* [18,22], we consider

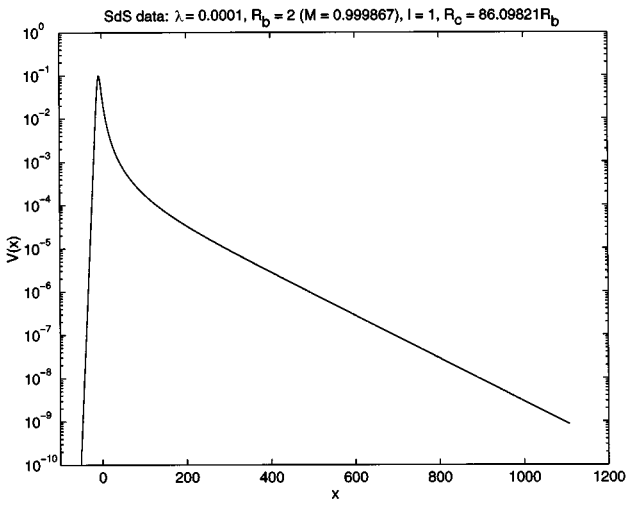

FIG. 7. Exponential decrease of the right side of $V(x)$ in the SdS background.

a spherically symmetric static metric of the form (2) with lapse function

$$N(r)=1-m\frac{(\ln|r|)^{\beta}}{r^{\alpha}}. \tag{23}$$

The constants α and β are integers, where $\beta\geqslant 0$ but $\alpha>0$. The other constant m is a real number. When we have $\alpha=1$, $\beta=0$, and $D=3$, this becomes a Schwarzschild background of mass $m/2$. Once we have the lapse function, we can compute the potential function

$$V_e(r)=\frac{(2l+D-3)(2l+D-1)}{4r^2}+m\frac{4\xi(D-1-\alpha)(D-2-\alpha)-(D-1)(D-3-2\alpha)}{4}\frac{(\ln|r|)^{\beta}}{r^{\alpha+2}}$$
$$+m\beta\frac{2\xi(2D-3-2\alpha)-D+1}{2}\frac{(\ln|r|)^{\beta-1}}{r^{\alpha+2}}+m\beta(\beta-1)\xi\frac{(\ln|r|)^{\beta-2}}{r^{\alpha+2}} \tag{24}$$

from Eq. (6).

We first find the static solution $\psi_S(r)$ of wave equation (7), by obtaining the solution of the equation $\mathcal{L}[\psi_S(r)]=0$. It is straightforward to show that $\psi_S(r)$ has the form

$$\psi_S(r)=r^{-\gamma}\sum_{j=0}^{\infty}\frac{a_j(r)}{r^{j\alpha}}+r^{\gamma+1}\sum_{j=0}^{\infty}\frac{c_j(r)}{r^{j\alpha}}, \tag{25}$$

where $\gamma\equiv l+(D-3)/2$. Notice that γ is an integer when the spatial dimension D is odd. Except when $D=1$ this integer is always positive. Hence it is the first sum of the solution that is physically relevant since it vanishes for large r, and we choose this as the static solution. For the remainder of this section, we assume that $D\geqslant 3$ so that this choice of $\psi_S(r)$ is valid. The coefficients $a_0(r)$ and $c_0(r)$ are arbitrary constants but the other coefficients are all polynomial in $\ln|r|$. The generating equations for $a_j(r)$ and $c_j(r)$ are given in the Appendix.

We follow the approach in Refs. [9,23] and let

$$\psi_I=\sum_{i=0}^{\infty}B_i(r)[g^{(-i)}(u)+(-1)^i f^{(-i)}(v)] \tag{26}$$

be the form of the initial wave, i.e., the wave emitted by a star at the onset of gravitational collapse. In other words, this is the time when $t\ll r$. The functions $g(u)$ and $f(v)$ are as yet unknown. The term $g^{(-i)}(u)$ represents i integrations of the function $g(u)$ with respect to u; similarly for $f^{(-i)}(v)$. Using Eq. (26), Eq. (11) becomes

$$0=\frac{1}{2}N(r)\frac{d}{dr}B_0(r)[g^{(1)}(u)-f^{(1)}(v)]$$
$$-\frac{1}{4}N(r)\sum_{i=0}^{\infty}\left\{\mathcal{L}[B_i(r)]-2\frac{d}{dr}B_{i+1}(r)\right\}$$
$$\times[g^{(-i)}(u)+(-1)^i f^{(-i)}(v)]. \tag{27}$$

This equation has a set of solutions

$$B_0(r)=1, \tag{28}$$

$$B_{i+1}(r)=\frac{1}{2}N(r)\frac{d}{dr}B_i(r)-\frac{1}{2}\int V_e(r)B_i(r)dr,$$

$$i=0,1,2,\ldots, \tag{29}$$

where we have set $B_0(r)=$ const $=1$ without loss of generality. The pair of equations above allows us to generate $B_i(r)$ hierarchically in a straightforward manner.

We can split each $B_i(r)$ into two parts, denoted by $B_i^P(r)$ and $B_i^T(r)$. $B_i^P(r)$ is defined as the m-independent portion of $B_i(r)$, while $B_i^T(r)$ is the rest, which is m dependent. Physically, the part $B_i^P(r)$ represents the wave on the light cone because it is the part that would be generated if the background were flat ($m=0$). Price referred to this part as the primary wave which depends only on the mode of the spherical harmonics. The other part $B_i^T(r)$ is called the tail of the wave because it is created by the presence of the spacetime curvature and is off the light cone due to scattering. Given Eqs. (28) and (29), one can show that the primary part of $B_i(r)$ is simply

$$B_i^P(r)=\frac{\Gamma(\gamma+1+i)}{2^i i!\Gamma(\gamma+1-i)r^i}. \tag{30}$$

When D is odd, γ is an integer and the sequence $\{B_i^P(r)\}_{i=0}$ truncates. However, if D is even, the sequence does not terminate and the primary part of the initial wave ψ_I has infinitely many terms. Indeed, when this is the case, it is inappropriate to call $B_i^P(r)$ the primary part because there are tails present. The approach breaks down because the primary and tail parts of the wave become indistinguishable. This is the reason we restrict ourselves to odd D in this section as mentioned earlier.

Let us now consider the tail part of $B_i(r)$. Unlike the primary part, $B_i^T(r)$ has no simple solution. Fortunately one can always generate $B_i(r)$ recursively. Note that $B_i^T(r)$ is of order $O((\ln|r|)^{\beta}/r^{i+\alpha})$.

Since γ is an integer in odd spatial dimensions, it is convenient to define the functions $G(u)$ and $F(v)$ as

$$G(u)=g^{(-\gamma)}(u) \quad \text{and} \quad F(v)=f^{(-\gamma)}(v), \tag{31}$$

such that the initial wave can be expressed as $\psi_I=\Sigma B_i(r)T_I{}^{\gamma-i}(u,v)$, where

$$T_I{}^{\gamma-i}(u,v)\equiv G^{(\gamma-i)}(u)+(-1)^i F^{(\gamma-i)}(v). \tag{32}$$

When the background is flat ($m=0$), only the first $\gamma+1$ terms of $B_i^P(r)$ survive. We expect that any outgoing radiation will propagate to spatial infinity without any scattering in a flat background. Therefore we must have

$$F^{(\gamma)}(v)=F^{(\gamma-1)}(v)=\cdots=F^{(1)}(v)=F^{(0)}(v)=0 \quad (33)$$

because $F(v)$ represents the scattered infalling radiation and the $B_i^P(r)$ are nonzero only for $0\leqslant i\leqslant\gamma$. In other words, we insist that $F(v)=0$.

For concreteness, we suppose the scalar wave starts leaving the star at retarded time $u=U_0$; that is to say, the scalar field is zero before $u=U_0$. Continuity then implies

$$G^{(\gamma)}(U_0)=G^{(\gamma-1)}(U_0)=\cdots=G^{(1)}(U_0)=G^{(0)}(U_0)=0, \quad (34)$$

$$G^{(-1)}(u)=\int_{U_0}^{u}G^{(0)}(\zeta)d\zeta,$$

$$G^{(-2)}(u)=\int_{U_0}^{u}G^{(-1)}(\zeta)d\zeta,\ \ldots\ . \quad (35)$$

We also assume that there is essentially no emission from the star after $u=U_1>U_0$ (due to gravitational red shift). When the star possesses no initial static moment at the onset of collapse, this cutoff condition is translated into

$$G^{(\gamma)}(u)=G^{(\gamma-1)}(u)=\cdots=G^{(1)}(u)=G^{(0)}(u)=0,$$

$$\forall u\geqslant U_1>U_0, \quad (36)$$

because only the terms $G(u)$ to $G^{(\gamma)}(u)$ which represent the primary wave correspond to the emission from the star. This condition implies

$$G^{(-1)}(u)=\int_{U_0}^{u}G^{(0)}(\zeta)d\zeta=\int_{U_0}^{U_1}G^{(0)}(\zeta)d\zeta=\text{const},$$

$$\forall u\geqslant U_1. \quad (37)$$

Therefore, if there is no static moment before $u=U_0$, the scalar wave after time $u=U_1$ is

$$\psi_{u\geqslant U_1}=\sum_{i=\gamma+1}^{\infty}B_i(r){T_I}^{\gamma-i}(u,v), \quad (38)$$

where ${T_I}^{-1}(u,v)$ is only a constant and $B_i(r)=B_i^T(r)$ is of order $O((\ln|r|)^{\beta}/r^{i+\alpha})$. So the first term of this solution which is time independent is of order $O((\ln|r|)^{\beta}/r^{\gamma+\alpha+1})$. Physically, this says the tail of the perturbation persists after time $u=U_1$. The primary part of the wave has been ''washed out'' by the gravitational redshift before $u=U_1$.

The situation is more complicated if the star carries a static moment at the onset of the collapse because the static wave $\psi_S(r)$ can also be divided into primary and tail parts. In this case, we superimpose $\psi_S(r)$ of Eq. (25) and $\psi_I(r)$ of Eq. (26) together to form a new initial scalar wave. We also suppose that only the tail of the perturbation persists after the retarded time $u=U_1$ [9]. For the superimposed initial wave this cutoff condition requires

$$G^{(0)}(u)=-\frac{2^{\gamma}\gamma!}{(2\gamma)!},\quad \forall u\geqslant U_1\geqslant U_0, \quad (39)$$

which yields

$$G^{(\gamma)}(u)=G^{(\gamma-1)}(u)=\cdots=G^{(1)}(u)=0. \quad (40)$$

The restriction on $G(u)$ above ensures that the primary part of Eq. (26) can be canceled by the m-independent part of Eq. (25) properly after time U_1, leaving the combined ψ_I to be m dependent only after U_1. As a result, the wave with initial static moment will become

$$\psi_{u\geqslant U_1}=\frac{1}{r^{\gamma}}\sum_{j=1}^{\infty}\frac{a_j(r)}{r^{j\alpha}}+\sum_{i=\gamma}^{\infty}B_i^T(r){T_I}^{\gamma-i}(u,v). \quad (41)$$

One can show that the first sum in the equation above is of order $O((\ln|r|)^{\beta}/r^{\gamma+\alpha})$ because the coefficient function $a_1(r)$ is a polynomial in $\ln|r|$ with degree β. In the second sum, the term ${T_I}^0(u,v)$ is a constant which equals to $G(u)$, and $B_{\gamma}^T(r)$ is of order $O((\ln|r|)^{\beta}/r^{\gamma+\alpha})$. Therefore, instead of having a time-independent part of order $O((\ln|r|)^{\beta}/r^{\gamma+\alpha+1})$, the wave with initial static moment has an order $O((\ln|r|)^{\beta}/r^{\gamma+\alpha})$ only.

Now we turn our attention to the scalar wave at late time. By late time, we mean $t\gg r$. For the late time wave ψ_L, we introduce another ansatz

$$\psi_L=\sum_{i=0}^{\infty}C_i(r)T_L^i(u,v),$$

$$T_L^i(u,v)\equiv I^{(i)}(u)+(-1)^iH^{(i)}(v). \quad (42)$$

By substituting $\psi=\psi_L$, Eq. (11) becomes

$$\frac{1}{4}N(r)\mathcal{L}[C_0(r)]T_L^0(u,v)$$

$$+\frac{1}{4}N(r)\sum_{i=0}^{\infty}\left\{\mathcal{L}[C_{i+1}(r)]-2\frac{d}{dr}C_i(r)\right\}$$

$$\times T_L^{i+1}(u,v)=0. \quad (43)$$

This equation has another set of solutions

$$\mathcal{L}[C_0(r)]=0, \quad (44)$$

$$\mathcal{L}[C_{i+1}(r)]=2\frac{d}{dr}C_i(r),\quad i=0,1,2,\ldots\ . \quad (45)$$

Unlike the case for the initial wave ψ_I [for which the functions $B_i(r)$ can be calculated recursively using straightforward differentiation and integration], recursive generation of the functions $C_i(r)$ involves inverting the differential operator $\mathcal{L}$. The zero order equation has a solution

$$C_0(r)=r^{\gamma+1}\sum_{j=0}^{\infty}\frac{c_j(r)}{r^{j\alpha}}. \quad (46)$$

The coefficient functions $c_j(r)$ are those in Eq. (25). They can be calculated by using the generating equations in the

Appendix. The other inhomogeneous differential equation (45) has a solution of the form

$$C_i(r)=r^{\gamma+1+i}\sum_{j=0}^{\infty}\frac{c_j^i(r)}{r^{j\alpha}}, \tag{47}$$

where $i=0,1,2,\ldots$. When $i=0$, it is understood that $c_j^0(r)=c_j(r)$. The coefficients $c_j^i(r)$ are also given in the Appendix. Since each coefficient $c_0^i(r)$ is a constant instead of a polynomial in $\ln|r|$, we can estimate the order of the late time wave ψ_L as

$$\psi_L=\sum_{i=0}^{\infty}O(r^{\gamma+1+i}){T_L}^i(u,v). \tag{48}$$

Finally we match the late time solution to the initial solution at some transient period where u, v, and r are of the same order. As the background is asymptotically flat, the tortoise coordinate x must have an order similar to that of r in this transient region. That is to say, the orders of r and t are the same. The initial wave $\psi_{u\geqslant U_1}$ in this period becomes

$$\psi_{u\geqslant U_1}=O\left(\frac{(\ln|r|)^{\beta}}{r^{\gamma+\alpha+1}}\right)\text{without an initial static moment,}$$

$$\psi_{u\geqslant U_1}=O\left(\frac{(\ln|r|)^{\beta}}{r^{\gamma+\alpha}}\right)\quad\text{with an initial static moment.}$$

In order to have consistent orders in the transient period, we must have

$${T_L}^0(t,t)\sim O\left(\frac{(\ln|t|)^{\beta}}{t^{2\gamma+2+\alpha}}\right) \tag{49}$$

if the star has no initial static moment, while the order of ${T_L}^0$ must be

$${T_L}^0(t,t)=O\left(\frac{(\ln|t|)^{\beta}}{t^{2\gamma+1+\alpha}}\right) \tag{50}$$

if the star has a static moment at the onset of collapse. In other words, Eqs. (49) and (50) give the falloff behavior of the wave at late time. The inverse power falloff behavior modified by a logarithmic term was first noted by Ching *et al.* [22]. For a Schwarzschild background, we set $D=3$, $\alpha=1$, and $\beta=0$ and have $\gamma=l$, yielding the familiar power-law decay rate [9,23].

IV. 3D BLACK HOLE BACKGROUND

The $(2+1)$-dimensional black hole spacetime obtained by Banados, Teitelboim, and Zanelli [19] is a spacetime which satisfies the vacuum Einstein equations with a negative cosmological constant ($\Lambda<0$). Its metric is

$$ds^2=-N(r)dt^2+\frac{dr^2}{N(r)}+r^2\left(-\frac{J}{2r^2}dt+d\phi\right)^2, \tag{51}$$

$$N(r)=|\Lambda|r^2-M+\frac{J^2}{4r^2}, \tag{52}$$

and is actually anti–de Sitter spacetime with identifications. The constant $M>0$ is the quasilocal mass of the black hole and J is the angular momentum of the hole [24]. For our purposes we shall regard the above metric as a spacetime which is an asymptotically anti–de Sitter spacetime.

When $J=0$, the wave equation (1) gives Eq. (10) with

$$V_e(r)=\frac{3|\Lambda|}{4}(1-8\xi)+\frac{M+4l^2}{4r^2}. \tag{53}$$

In this case, the tortoise coordinate x is given by

$$x\equiv\int\frac{dr}{N(r)}=\frac{1}{2\sqrt{|\Lambda|M}}\ln\left|\frac{\sqrt{|\Lambda|}r-\sqrt{M}}{\sqrt{|\Lambda|}r+\sqrt{M}}\right|. \tag{54}$$

As r goes from $\sqrt{M/|\Lambda|}$ to infinity, the tortoise coordinate has a range $(-\infty,0)$. Thus we can write r in terms of x as

$$r=\sqrt{\frac{M}{|\Lambda|}}\frac{1+\exp(2\sqrt{|\Lambda|M}x)}{1-\exp(2\sqrt{|\Lambda|M}x)}. \tag{55}$$

For conformal wave in $2+1$ dimensions, the parameter ξ equals 1/8 and the potential barrier V becomes

$$V(x)=V_0\frac{\exp(2\lambda x)}{[1+\exp(2\lambda x)]^2}, \tag{56}$$

where, for convenience, we have defined

$$V_0\equiv|\Lambda|(M+4l^2)>0\quad\text{and}\quad\lambda\equiv\sqrt{|\Lambda|M}>0. \tag{57}$$

The procedure for finding a solution to the conformal scalar wave equation is as follows. We first write down the representation of the solution ψ in terms of Green's functions. The rest of the problem then reduces to that of looking for the correct Green's function. We will Fourier transform from the time domain to the frequency domain and obtain the Green's function in frequency space. Once we have the Green's function in frequency domain, an inverse Fourier transformation will yield the solution $\psi(t,x)$. A case when $J\neq0$ will be studied as well.

We first assume that there exists a Green's function

$$G(x,\xi;t-\tau)=G(\xi,x;t-\tau), \tag{58}$$

which is zero when $t<\tau$. We define an operator D as

$$D=\partial_{tt}-\partial_{xx}+V(x), \tag{59}$$

such that the Green's function with respect to this operator has the property

$$DG(x,\xi;t-\tau)=[\partial_{tt}-\partial_{xx}+V(x)]G(x,\xi;t-\tau)=\delta(t-\tau)\,\delta(x-\xi). \tag{60}$$

The inner product between $D\psi(t,x)$ and $G(x,\xi;t-\tau)$ gives

$$\psi(t,x)=\int_{-\infty}^{0}[G(x,\xi;t)\partial_t\psi(0,\xi)+\psi(0,\xi)\partial_t G(x,\xi;t)]d\xi + \int_{0}^{\infty}[G(x,\xi;t-\tau)\partial_\xi\psi(\tau,\xi) - \psi(\tau,\xi)\partial_\xi G(x,\xi;t-\tau)]_{\xi=-\infty}^{\xi=0}d\tau. \quad (61)$$

As a result, we have changed the question from looking for $\psi(t,x)$ to searching for an appropriate Green's function.

We now carry out a Fourier transformation and define

$$\tilde{G}(x,\xi;\omega)=\int_{-\infty}^{\infty}G(x,\xi;t)\exp(i\omega t)dt. \quad (62)$$

Therefore Eq. (60) becomes

$$\tilde{D}\tilde{G}(x,\xi;\omega)=[-\omega^2-\partial_{xx}+V(x)]\tilde{G}(x,\xi;\omega)=\delta(x-\xi) \quad (63)$$

if the Green's function $G(x,\xi;t)$ satisfies the conditions

$$\lim_{t\to\infty}G(x,\xi;t)=\lim_{t\to\infty}\partial_t G(x,\xi;t)=0. \quad (64)$$

On physical grounds these assumptions are reasonable because any localized quantity is expected to be dispersed throughout the space by means of wave propagation. Mathematically, these assumptions are consistent with the Fourier transformability of the function $G(x,\xi;t)$ which must be absolutely integrable over $\Re$ in order for $\tilde{G}(x,\xi;\omega)$ to be well defined. The Green's function in frequency space can be represented as

$$\tilde{G}(x,\xi;\omega)=\begin{cases}\dfrac{f(\xi;\omega)g(x;\omega)}{W(\omega;g,f)} & \text{if} \quad \xi<x,\\[2ex] \dfrac{f(x;\omega)g(\xi;\omega)}{W(\omega;g,f)} & \text{if} \quad x<\xi,\end{cases} \quad (65)$$

where the function $W(\omega;g,f)$ is the Wronskian of two linearly independent functions $f(x;\omega)$ and $g(x;\omega)$, that is,

$$W(\omega;g,f)=g(x;\omega)\partial_x f(x;\omega)-f(x;\omega)\partial_x g(x;\omega). \quad (66)$$

The functions $f(x;\omega)$ and $g(x;\omega)$ are two independent solutions of the equations

$$\tilde{D}f(x;\omega)=\tilde{D}g(x;\omega)=0, \quad (67)$$

so that $W(\omega;g,f)$ is independent of x.

Let $\tilde{\psi}(x;\omega)$ be the Fourier transformation of the solution $\psi(t,x)$. We impose boundary conditions on the functions $f(x;\omega)$ and $g(x;\omega)$ so that

$$f(x;\omega)\propto\tilde{\psi}(x;\omega) \quad \text{and} \quad \partial_x f(x;\omega)\propto\partial_x\tilde{\psi}(x;\omega) \quad (68)$$

at the point $x\to-\infty$. At the other end ($x=0$) we insist that

$$g(x;\omega)\propto\tilde{\psi}(x;\omega) \quad \text{and} \quad \partial_x g(x;\omega)\propto\partial_x\tilde{\psi}(x;\omega). \quad (69)$$

In Eq. (61), after we have used the inverse Fourier transformation and interchanged the integrals with respect to $d\omega$ and $d\tau$, the representation of $\psi(t,x)$ simply becomes

$$\psi(t,x)=\int_{-\infty}^{0}[G(x,\xi;t)\partial_t\psi(0,\xi)+\psi(0,\xi)\partial_t G(x,\xi;t)]d\xi. \quad (70)$$

A. Exact solution for static 3D black hole potential

We will obtain the exact solution for the scalar wave ψ corresponding to the potential barrier (56) in a static 3D black hole background. This entails finding the solution of the differential equation $\tilde{D}h(x;\omega)=0$. This equation has two solutions [25]: namely,

$$h_\pm(x;\omega)=\exp(\pm i\omega x)F(-\nu,1+\nu;1\pm\mu;z(x)), \quad (71)$$

$$z(x)=\frac{\exp(2\lambda x)}{1+\exp(2\lambda x)}, \quad (72)$$

$$\mu=i\frac{\omega}{\lambda}, \quad (73)$$

$$\nu=-\frac{1}{2}+i\frac{l}{\sqrt{M}}, \quad (74)$$

where F is the hypergeometric function. Because x goes from minus infinity to zero, z has a range of (0,1/2) which yields absolute convergence to the hypergeometric function [26]. At the boundary $x\to-\infty$ (the event horizon of the 3D black hole) we employ the condition

$$f(x;\omega)=\exp(-i\omega x), \quad x\to-\infty, \quad (75)$$

as usual [18]. Since this spacetime is an asymptotically anti–de Sitter spacetime instead of a flat spacetime, the boundary condition at spatial infinity is less trivial. Choosing the Dirichlet conditions [21]

$$g(x=0;\omega)=0 \quad \text{and} \quad \partial_x g(x;\omega)|_{x=0}=1, \quad (76)$$

the two functions $f(x;\omega)$ and $g(x;\omega)$ read

$$f(x;\omega)=h_-(x;\omega), \quad (77)$$

$$g(x;\omega)=h_+(x;\omega)-Ah_-(x;\omega), \quad (78)$$

where the coefficient A is given by

$$A\equiv\frac{h_+(0;\omega)}{h_-(0;\omega)} =2^{-2\mu}\frac{\Gamma(1+\mu)}{\Gamma(1-\mu)}\frac{\Gamma(1/2-[\mu+\nu]/2)}{\Gamma(1+[\mu+\nu]/2)}\frac{\Gamma(1-[\mu-\nu]/2)}{\Gamma(1/2+[\mu-\nu]/2)}. \quad (79)$$

The solution g is typically multiplied by a normalization factor, which we have set to unity since it is always canceled out once the Wronskian is taken into account. It is not difficult to show that the Wronskian of g and f is

$$W(\omega;g,f)=W(\omega;h_+,h_-)=-2i\omega. \tag{80}$$

Now we put everything together and obtain

$$\widetilde{G}(x,\xi<x;\omega)=\frac{i}{2\omega}h_-(\xi;\omega)[h_+(x;\omega)-Ah_-(x;\omega)]. \tag{81}$$

The remainder of the problem is to bring the Green's function from the frequency domain back to the time domain.

The inverse Fourier transformation is given by the equation

$$G(x,\xi;t)=\frac{1}{2\pi}\int_{-\infty}^{\infty}\widetilde{G}(x,\xi;\omega)\exp(-i\omega t)d\omega. \tag{82}$$

We evaluate this integral by analytically extending ω to complex values and using Cauchy's residue theorem. The contour of integration is chosen to be a large, closed semicircle on the lower half ω plane, with the center at $\omega=0$. We make an indentation consisting of a small semicircle centered at the origin because this point which is a pole from the Wronskian lies on the integration contour. By Jordan's lemma, the contribution from the arc of the large semicircle goes to zero as the radius of the arc tends to infinity. The Green's function then becomes

$$G(x,\xi;t)=i\sum \text{Res}\{\widetilde{G}(x,\xi;\omega)\exp(-i\omega t)\}, \tag{83}$$

where $\text{Res}\{k(z)\}$ denotes the residue of the function $k(z)$ at a pole. In our case, the poles of the Green's function $\widetilde{G}(x,\xi;\omega)$ within the contour come from the Γ functions of the coefficient A. That is to say, the poles correspond to

$$-k_1=1+\mu, \tag{84}$$

$$-k_2=\frac{1}{2}-\frac{\mu+\nu}{2}, \tag{85}$$

$$-k_3=1-\frac{\mu-\nu}{2}, \tag{86}$$

where k_1, k_2, and k_3 equal 0, 1, 2, 3, ... Notice that there are infinitely many poles on the lower half ω plane. Because there is no branch cut in either h_+ or h_-, we conclude that $G(x,\xi;t)$ decays to zero exponentially. The dominant exponential decaying rate is determined by the pole closest to the real axis on the lower half ω plane. According to the three equations above, there are two such poles, namely,

$$\omega=\pm\frac{l}{\sqrt{M}}\lambda-i\frac{3}{2}\lambda. \tag{87}$$

As a result, the exponentially decaying Green's function $G(x,\xi;t)$ implies that $\psi(t,x)$ also decays in this manner at a rate $\exp(-3\lambda t/2)$.

Had we chosen the Neumann condition instead of the Dirichlet condition for $g(x,\omega)$ [21], that is,

$$g(x=0;\omega)=1 \quad \text{and} \quad \partial_x g(x;\omega)\big|_{x=0}=0, \tag{88}$$

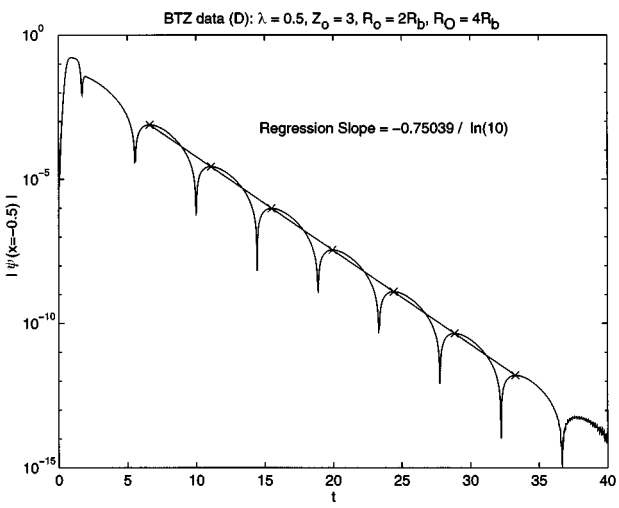

FIG. 8. Exponential falloff for a conformal scalar wave using Dirichlet boundary condition.

the function $g(x,\omega)$ would simply become

$$g(x;\omega)=h_+(x;\omega)-Bh_-(x;\omega), \tag{89}$$

where the coefficient constant B is defined as

$$B\equiv\frac{\partial_x h_+(0;\omega)}{\partial_x h_-(0;\omega)}$$
$$=2^{-2\mu}\frac{\Gamma(1+\mu)}{\Gamma(1-\mu)}\frac{\Gamma(-[\mu+\nu]/2)}{\Gamma(1/2+[\mu+\nu]/2)}\frac{\Gamma(1/2-[\mu-\nu]/2)}{\Gamma([\mu-\nu]/2)}. \tag{90}$$

The change from A to B causes the singular terms in $\widetilde{G}$ to become $\Gamma(1+\mu)$, $\Gamma(-[\mu+\nu]/2)$, and $\Gamma(1/2-[\mu+\nu]/2)$, which also have infinitely many poles on the lower half ω plane. A quick inspection shows that $\psi(t,x)$ also dies out to zero at an exponential rate of $\exp(-\lambda t/2)$ because the poles which are closest to the real axis are

$$\omega=\pm\frac{l}{\sqrt{M}}\lambda-i\frac{1}{2}\lambda. \tag{91}$$

The next few graphs are the numerical results using the potential (56). We used the same initial condition as in the numerical computation for the Schwarzschild case. Since the background is an asymptotically anti–de Sitter background, we integrate Eq. (10) numerically with the Dirichlet boundary condition at $r=\infty$ (i.e., $x=0$). Figures 8 and 9 illustrate the falloff behavior of the wave using different exponential potential functions. In both graphs, the initial Gaussian impulse is located at twice the black hole radius ($2R_b$) and the observation is made at $4R_b$. The straight line asymptote of the ringing behavior on the semilogarithmic graph corresponds to exponential falloff, numerically confirming that the wave exponentially decays in this asymptotically nonflat background at the rate of $\exp(-3\lambda t/2)$.

Figures 10 and 11 illustrate the numerical results using the Neumann boundary condition at $x=0$. It is clear from the two graphs that the scalar wave also exponentially decays when the Neumann condition is used. One can see that the

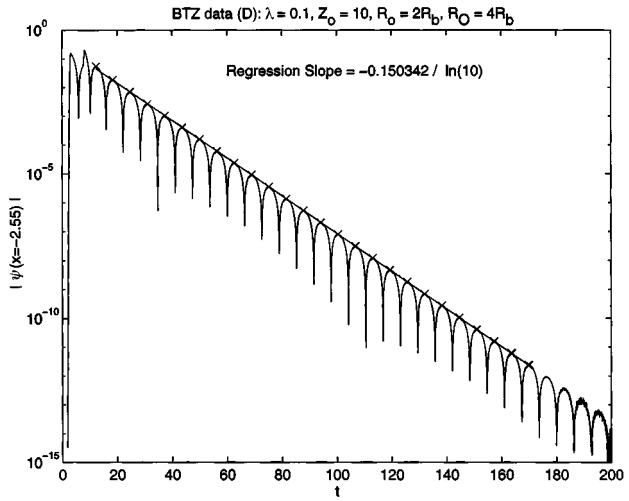

FIG. 9. Another semilogarithmic graph as in Fig. 8 but with different parameters.

falloff rate is 3 times slower than that in the Dirichlet cases because the dominant poles in this case are 3 times closer to the real ω axis than those in the Dirichlet cases.

B. Spinning 3D black hole background

When $J\neq 0$, i.e., when the black hole rotates, we also find a late time exponential decay rate, as we shall now demonstrate.

If we assume that

$$\Psi(t,r,\phi)=\frac{\psi(t,r)}{\sqrt{r}}, \tag{92}$$

that is to say, that there is no ''spherical harmonic'' component to the wave, the conformal scalar wave equation $\nabla^2\Psi=R\Psi/8$ will reduce to Eq. (10). The tortoise coordinate x is defined as before but the potential barrier becomes

$$V_e(x(r))=-\frac{3|\Lambda|}{4}+\frac{1}{2r}\partial_r N(r)-\frac{N(r)}{4r^2}. \tag{93}$$

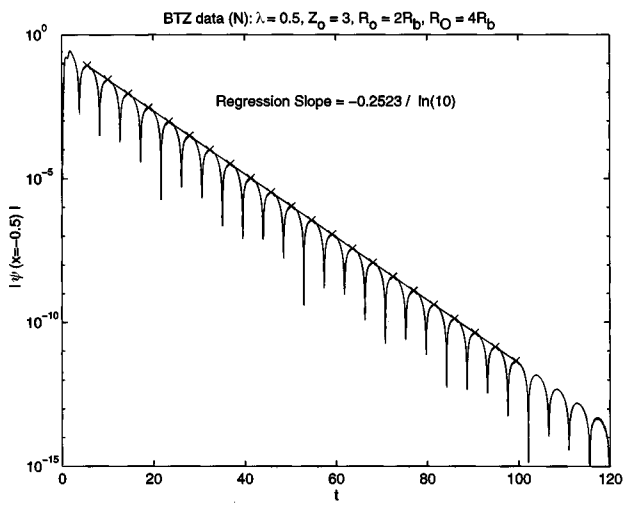

FIG. 10. Exponential falloff using the Neumann condition.

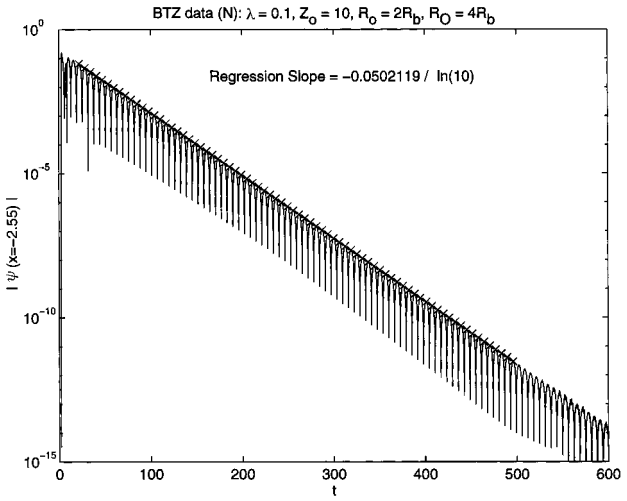

FIG. 11. The same as in Fig. 10 but with different parameters.

In this spinning case, the black hole has two horizons $R_\pm$ which are given by the equation

$$R_\pm^2=\frac{1}{2|\Lambda|}[M\pm\sqrt{M^2-|\Lambda|J^2}]. \tag{94}$$

The lapse function $N(r)$ can then be written in terms of R_+ and R_- as

$$N(r)=\frac{|\Lambda|}{r^2}(r^2-R_+^2)(r^2-R_-^2). \tag{95}$$

As a result, the tortoise coordinate reads

$$x(r)=\frac{1}{2|\Lambda|(R_+^2-R_-^2)}\left[R_+\ln\left(\frac{r-R_+}{r+R_+}\right)-R_-\ln\left(\frac{r-R_-}{r+R_-}\right)\right], \tag{96}$$

which has an inverse of the form

$$\frac{R_+}{r(x)}=\frac{Y}{1-\sigma^2}\sum_{n=0}^{\infty}a_n(\sigma)Y^{2n}, \tag{97}$$

$$\sigma=\frac{R_-}{R_+}<1, \tag{98}$$

$$Y=\frac{1-\exp(2\lambda x)}{1+\exp(2\lambda x)}<1, \tag{99}$$

$$\lambda=|\Lambda|R_+(1-\sigma^2)>0. \tag{100}$$

The coefficients $a_n(\sigma)$, which read

$$a_0(\sigma)=1,\quad a_1(\sigma)=-\sigma^2\frac{3-\sigma^2}{3(1-\sigma^2)^2}, \tag{101}$$

$$a_2(\sigma)=\sigma^4\frac{25-17\sigma^2+3\sigma^4}{15(1-\sigma^2)^4},$$

$$a_3(\sigma)=-\sigma^6\frac{1008-1039\sigma^2+368\sigma^4-45\sigma^6}{315(1-\sigma^2)^6},\ldots, \tag{102}$$

are of order $O(\sigma^{2n})$. If σ is small enough, we can employ the approximation

$$\frac{1}{r(x)} \approx \frac{Y}{R_+}. \tag{103}$$

If we substitute this approximation into the potential barrier $V(x)$, we will obtain

$$V(x) \approx \Lambda^2 \frac{(R_+^2 - R_-^2)(R_+^2 - 4R_-^2)}{R_+^2} \frac{\exp(2\lambda x)}{[1+\exp(2\lambda x)]^2} + 12\Lambda^2(2R_+^2 - 3R_-^2)\frac{R_-^2}{R_+^2}\frac{\exp(4\lambda x)}{[1+\exp(2\lambda x)]^4} + 80\Lambda^2 \frac{R_-^4}{R_+^2}\frac{\exp(6\lambda x)}{[1+\exp(2\lambda x)]^6}. \tag{104}$$

It is obvious that the first term in the potential function above has a form identical to the potential function in the nonspinning 3D black hole case. Since $\lambda > 0$ but $x < 0$, the second term in the potential is always weaker than the first one. As a result we may iteratively solve the wave equation, treating the first term as the lowest order potential, the second term as the first correction to this approximation, and so on.

For clarity, we define

$$V_0(x) \equiv \Lambda^2 \frac{(R_+^2 - R_-^2)(R_+^2 - 4R_-^2)}{R_+^2} \frac{\exp(2\lambda x)}{[1+\exp(2\lambda x)]^2}, \tag{105}$$

$$V_1(x) \equiv 12\Lambda^2(2R_+^2 - 3R_-^2)\frac{R_-^2}{R_+^2}\frac{\exp(4\lambda x)}{[1+\exp(2\lambda x)]^4}, \tag{106}$$

$$\widetilde{D} \equiv -\omega^2 - \partial_{xx} + V_0(x) + V_1(x), \tag{107}$$

$$\widetilde{D}_0 \equiv -\omega^2 - \partial_{xx} + V_0(x). \tag{108}$$

Therefore the equation $\widetilde{D} f(x;\omega) = 0$ has a representation

$$f(x;\omega) = f_0(x;\omega) + \int_{-\infty}^{x} \frac{U_+(x)U_-(\xi) - U_-(x)U_+(\xi)}{W(\omega;U_-,U_+)} \times V_1(\xi) f(\xi;\omega) d\xi \tag{109}$$

at $x = -\infty$. The functions $U_+(x)$ and $U_-(x)$ satisfy the equation $\widetilde{D}_0 U_+(x) = \widetilde{D}_0 U_-(x) = 0$. The other function $f_0(x;\omega)$ satisfies the same equation as $U_+(x)$ and $U_-(x)$ and also satisfies the Dirichlet boundary conditions at $x \to -\infty$. In other words, $f_0(x;\omega)$ is the solution (77) in our case with different values of λ, μ, and ν and $U_\pm$ are $h_\pm$. Similarly the solution around $x = 0$ is

$$g(x;\omega) = g_0(x;\omega) - \int_{x}^{0} \frac{U_+(x)U_-(\xi) - U_-(x)U_+(\xi)}{W(\omega;U_-,U_+)} \times V_1(\xi) g(\xi;\omega) d\xi, \tag{110}$$

where $g_0(x;\omega)$ is just Eq. (78). We first compute the Wronskian $W(\omega;g,f)$ for $f(x;\omega)$ and $g(x;\omega)$ above. Since this Wronskian is x independent, the simplest way to compute it is to evaluate the quantity at the point $x = 0$. It is not difficult to show that

$$W(\omega;g,f) = W(\omega;g_0,f_0) + W(\omega;g_0,f)(x)\big|_{x=-\infty}^{x=0} = W(\omega;g_0,f_0) - W(\omega;g,f_0)(x)\big|_{x=-\infty}^{x=0}. \tag{111}$$

Since $g(x;\omega)$ and $f(x;\omega)$ satisfy a differential equation which differs from that satisfied by $g_0(x;\omega)$ and $f_0(x;\omega)$, the Wronskians $W(\omega;g_0,f)$ and $W(\omega;g,f_0)$ are functions of x in general. Therefore the correction $V_1(x)$ in the potential barrier induces an extra (x-independent) term in the Wronskian $W(\omega;g,f)$.

The first Born approximations for $f(x;\omega)$ and $g(x;\omega)$ read

$$f(x;\omega) \approx f_1(x;\omega) = f_0(x;\omega) - \frac{i}{2\omega}\int_{-\infty}^{x} [h_+(x)h_-(\xi) - h_-(x)h_+(\xi)] V_1(\xi) f_0(\xi) d\xi, \tag{112}$$

$$g(x;\omega) \approx g_1(x;\omega) = g_0(x;\omega) + \frac{i}{2\omega}\int_{x}^{0} [h_+(x)h_-(\xi) - h_-(x)h_+(\xi)] V_1(\xi) g_0(\xi) d\xi. \tag{113}$$

As a result, the Wronskian $W(\omega;g,f)$ can be approximated by

$$W(\omega;g,f) \approx W(\omega;g_0,f_0) + W(\omega;g_0,f_1)(x)\big|_{-\infty}^{0} = W(\omega;g_0,f_0) + \int_{-\infty}^{0} g_0(x;\omega) f_0(x;\omega) V_1(x) dx. \tag{114}$$

Since there are poles in the lower half ω plane in the Green's function $\widetilde{G}$ but there are no branch cuts in either f_1 or g_1, this implies that there is an exponentially decaying quasinormal ringing effect in the wave tail in this rotating 3D black hole configuration.

Figure 12 is the graph of the potential functions of this spinning case with zero angular harmonic. One can show that when the ratio $|\Lambda| J^2/M^2 > 16/25$, V_e becomes negative for some $r > R_+$. This behavior is illustrated in Fig. 12, where $V(x)$ becomes negative when $|x|$ is sufficiently large. In Fig. 13, we can see that the potential functions in both cases vanish at an exponential rate towards the event horizon. As usual, we put a Gaussian impulse at a distance twice that of the outer horizon, R_+, and the numerical response of the scalar waves over time at a distance $4R_+$ is shown in Fig. 14. This figure shows an exponential decay of the wave although its appearance differs from the previous graphs because there are no angular harmonics (i.e., $l = 0$). Indeed, if we set $l = 0$ in the static 3D black hole case, we find that the falloff also looks like that in Fig. 14 because the pole that is closest to the real ω axis for the Green's function in the frequency domain has no real part [Eqs. (87) and (91)].

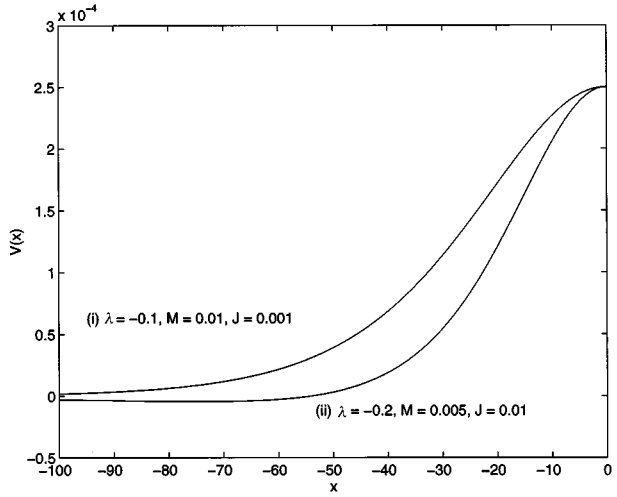

FIG. 12. Potential function $V(x)$ of two spinning 3D black hole backgrounds with (i) $|\Lambda|J^2/M^2=10^{-3}$ and (ii) $|\Lambda|J^2/M^2=0.8$.

V. SCHWARZSCHILD–ANTI-de SITTER BACKGROUND

Since the 3D black hole spacetime is an asymptotically anti–de Sitter spacetime, one might expect that the late time falloff behavior of any scalar wave in a Schwarzschild–anti-de Sitter (SAdS) background has similar behavior. In fact, the situation is quite different from the 3D case, in part because of the different dimensionality and in part because it is not possible to solve the wave equation (10) exactly in this background. Although the potential function $V_e(r)$ in this case reads

$$V_e(r)=\frac{2|\Lambda|}{3}(1-6\xi)+\frac{l(l+1)}{r^2}+\frac{2M}{r^3}, \tag{115}$$

which is quite similar to Eq. (53) in the 3D case, we cannot write r as a function of x in a closed form. That is to say, given the lapse function

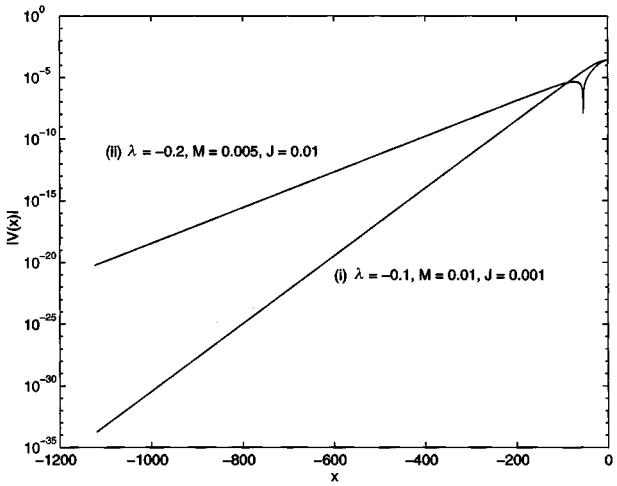

FIG. 13. Decaying exponential behavior of $|V(x)|$ near the black hole event horizon.

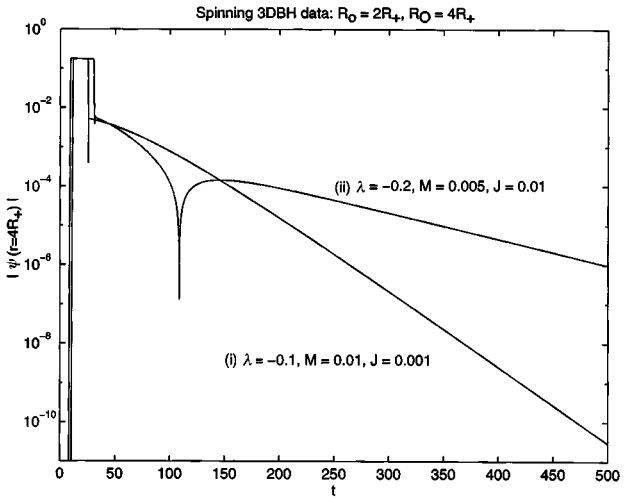

FIG. 14. Exponential decay of conformal scalar waves in spinning 3D black hole geometry.

$$N(r)=\frac{|\Lambda|}{3}r^2+1-\frac{2M}{r}=\frac{|\Lambda|}{3}r^2+1-\frac{R_b(3+|\Lambda|R_b^2)}{3r}, \tag{116}$$

where $\Lambda<0$ and the black hole radius R_b satisfies the equation $N(R_b)=0$, the tortoise coordinate

$$x=\frac{R_b}{2(1+|\Lambda|R_b^2)}\ln\left|\frac{(r-R_b)^2}{r^2+R_br+R_b^2+3/|\Lambda|}\right|$$
$$+\frac{\sqrt{3}(2+|\Lambda|R_b^2)}{\sqrt{|\Lambda|}(1+|\Lambda|R_b^2)\sqrt{4+|\Lambda|R_b^2}}$$

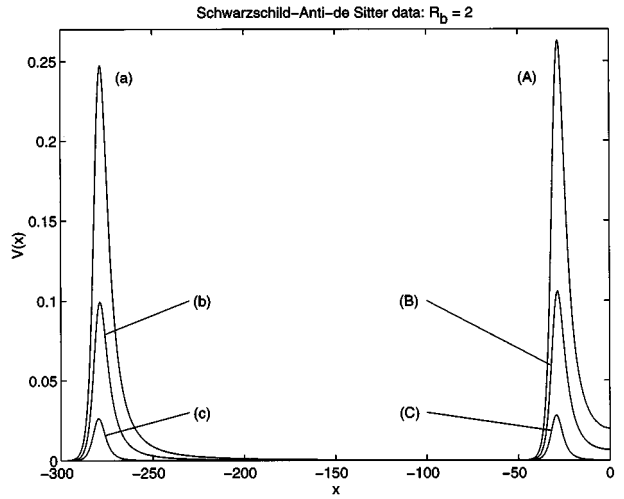

FIG. 15. Potential functions $V(x)$ for the SAdS background. The six potentials are generated with the parameters (a) $\Lambda=-10^{-4}$, $l=2$, (b) $\Lambda=-10^{-4}$, $l=1$, (c) $\Lambda=-10^{-4}$, $l=0$, (A) $\Lambda=-10^{-2}$, $l=2$, (B) $\Lambda=-10^{-2}$, $l=1$, and (C) $\Lambda=-10^{-2}$, $l=0$.

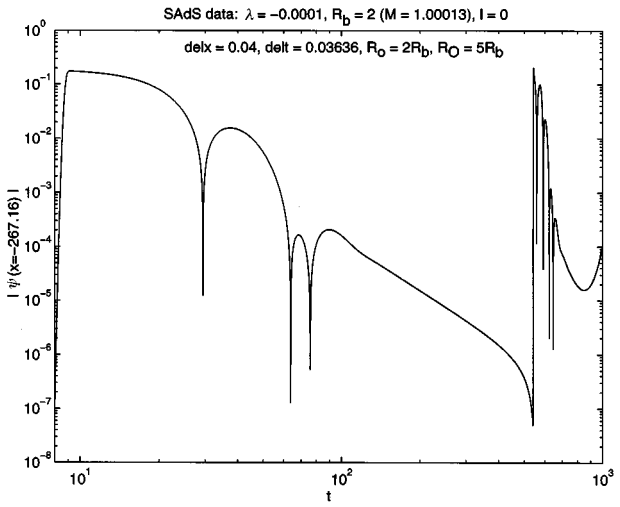

FIG. 16. Scalar wave of $l=0$ decays away in the SAdS background using the Dirichlet condition at $x=0$.

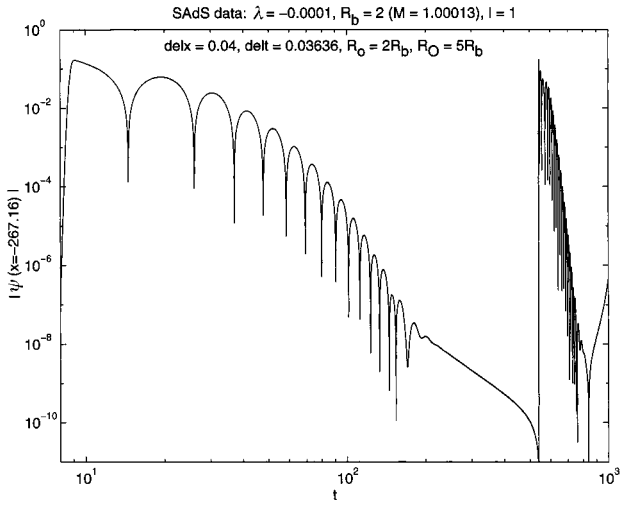

FIG. 18. Log-log graph of the decay behavior in the SAdS background using $l=1$ and the Dirichlet condition.

$$\times\left[\arctan\left(\frac{\sqrt{|\Lambda|}(2r+R_b)}{\sqrt{3}\sqrt{4+|\Lambda|R_b^2}}\right)-\frac{\pi}{2}\right] \tag{117}$$

has no closed form inverse, and so we are unable to write down an explicit expression for the potential $V(x)$.

For the remainder of this section we set $\xi=1/6$ (i.e., we consider a conformal scalar field propagating on an SAdS background).

The most important difference between the 3D black hole background and SAdS background is the shape of the potential function $V(x)$. In both cases the potential functions are decreasing in an exponential manner toward the horizon. In the 3D case (either spinning or static) this function attains a maximum at a distance $r=\infty$ $(x=0)$. When the background is SAdS, this is no longer true because spatial infinity (which is still given by $x=0$) is not the place at which $V(x)$ has an absolute maximum (for $x\in\Re^-$). As with the Schwarzschild black hole (Fig. 2), the potential function $V(x)$ attains a maximum not far away from the event horizon. In the SAdS case, the shape of the potential function $V(x)$ is given in Fig. 15. Unlike the Schwarzschild case, the tortoise coordinate x for the SAdS background is bounded above. Eventually all the outgoing waves that leave the black hole region will return towards it due to the boundary condition at $x=0$. The returning wave will then reflect off of the potential barrier back toward spatial infinity. This is completely different behavior from the 3D case, in which the incoming wave from spatial infinity $x=0$ continues its journey to the black hole unhindered.

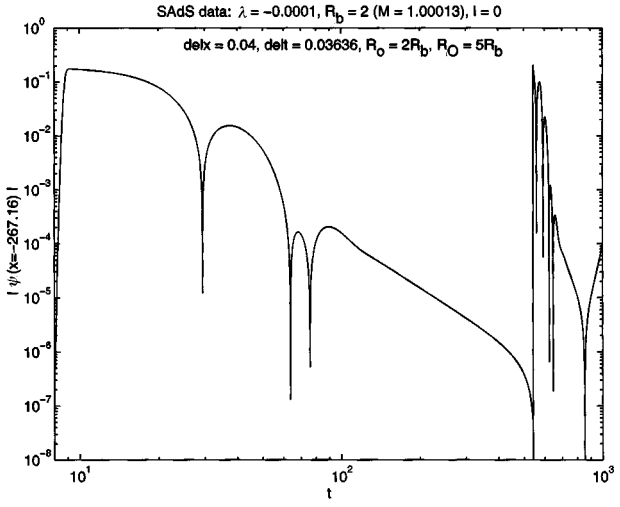

FIG. 17. Scalar wave falloff pattern of $l=0$ using the Neumann condition spatial infinity.

We can see from Fig. 15 that when $|\Lambda|$ is small [barriers (a)–(c)], the barrier maximum moves to the left, lengthening the traveling time from this maximum to spatial infinity. When l vanishes [cases (c) and (C)], $V(0)=0$ because $V(0)=l(l+1)|\Lambda|/3$ in general. Therefore barriers (a) and (b) have $V(0)\neq 0$ although this feature is not apparent on the graph due to the small size of $|\Lambda|$. The barrier height is considerably higher than the magnitude of $V(x)$ at $x=0$, and this feature becomes more pronounced for large l. This causes the scalar wave to bounce back and forth in the region outside the barrier. However, part of the scalar wave can surmount the barrier (thereby going into the black hole) because the barrier height is still finite. However, it takes a long time for a significant portion of the wave to enter the black hole.

We solve the wave equation in this SAdS background numerically. The results of the numerical integration of Eq. (10) using Eqs. (115) and (116) are given in the next few graphs. Figures 16 and 17 show the falloff behavior of a conformal scalar wave with $l=0$ initially located at a distance $r=2R_b$. The computation for Fig. 16 uses the Dirichlet condition at $x=0$ but Neumann boundary condition is employed for Fig. 17. Since the cosmological constant $|\Lambda|$ was chosen to be relatively small in both cases, namely, $|\Lambda|=10^{-4}$, we can see on both graphs that there is clearly an inverse power-decay behavior. According to the graph, this power-decay rate is roughly t^{-3} which agrees with the one in

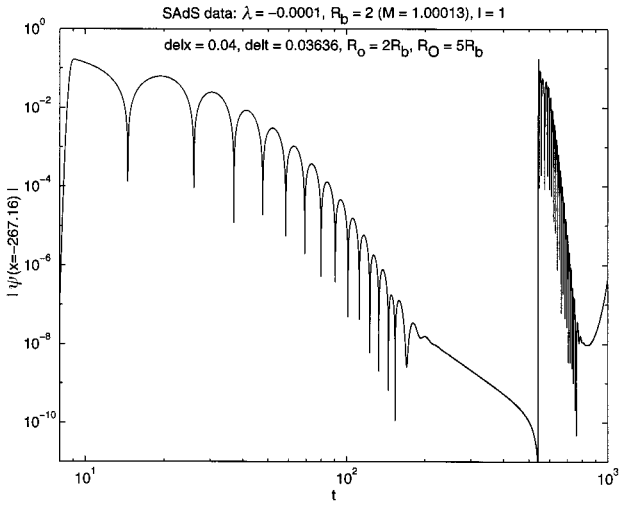

FIG. 19. Similar graph to Fig. 18 but using the Neumann condition.

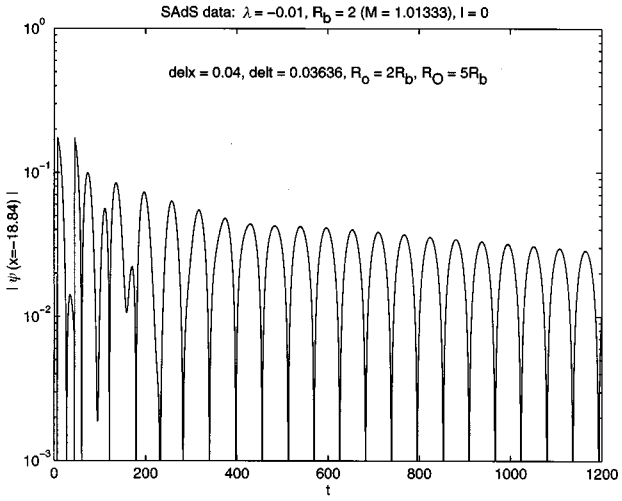

FIG. 21. Conformal scalar wave decay behavior using $l=0$ and the Neumann condition.

the Schwarzschild case. However, this inverse power decay does not last very long after the return of the outgoing wave from spatial infinity. Both diagrams show this returning wavefront.

For small $|\Lambda|$ and nonzero l, the falloff behavior resembles the case of $l=0$. Initially there is a ringing effect (due to the quasinormal modes) followed by inverse power-decay behavior as shown in Figs. 18 and 19.

Since the finite height of the potential maximum allows the scalar wave to surmount the barrier and leave the trapped region which is the exterior outside the barrier maximum, we expect that the peak value of the second returning wave is smaller than that of the first wave. However, it is unclear from simple inspection of Figs. 16 to 19 whether or not this is the case. Figures 20–23 are the numerical results we obtained using the potential functions (A) and (C) in Fig. 15. We compute the large $|\Lambda|$ case with both Dirichlet (Figs. 20 and 22) and Neumann (Figs. 21 and 23) boundary conditions. For this case there are more returning waves in a reasonable amount of CPU time. From these graphs, we can see that the scalar wave does indeed decrease but over a much larger time scale. Figures 20 and 21 indicate that the peak height has an approximate exponential falloff for $l=0$. For $l>0$, the peak height has a more complicated behavior illustrated in Figs. 22 and 23. Over long time scales the maximum peak height has a very mild approximate exponential falloff.

VI. CONCLUSION

The results of this work indicate clearly that the asymptotics of a given spacetime have a considerable influence on the late time falloff behavior of a scalar wave. The early work of Price showing that waves in a Schwarzschild background decay away according to an inverse power rate was recently extended by Ching *et al.* who found that the inverse

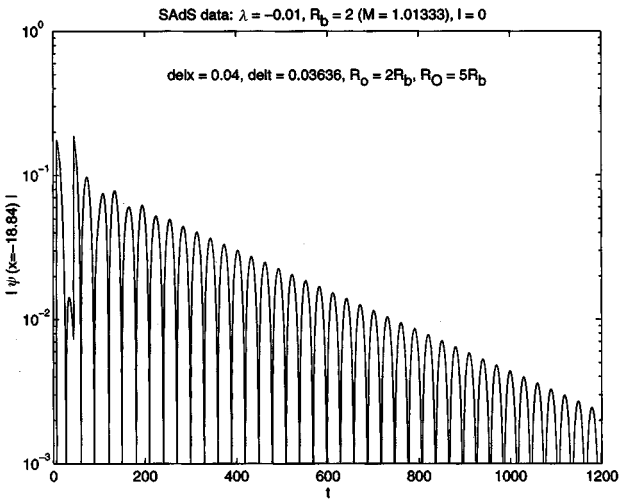

FIG. 20. Semilogarithmic graph of the decay behavior in the SAdS background using $l=0$ and the Dirichlet condition.

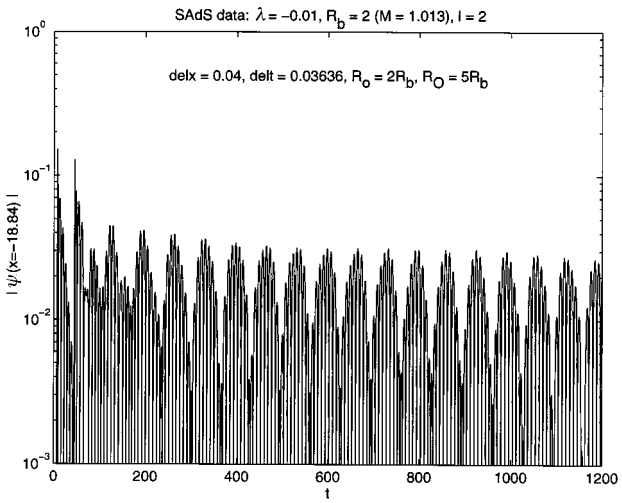

FIG. 22. Semilogarithmic graph of the decay behavior using nonzero l and the Dirichlet condition.

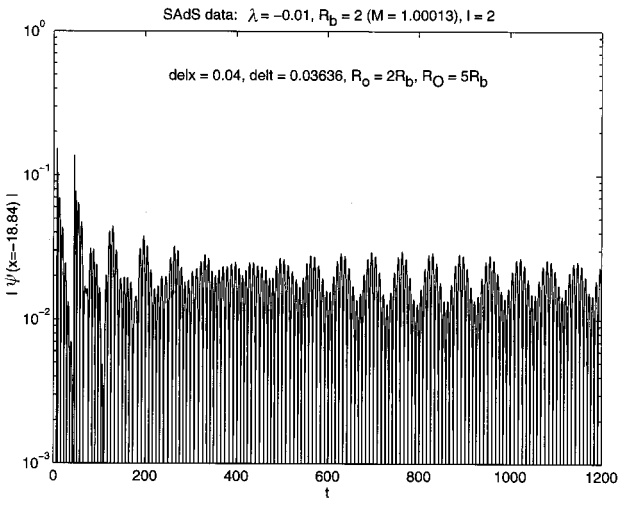

FIG. 23. This semilogarithmic graph is the Neumann analogue of Fig. 22.

power law can also be modified by a logarithmic term in some black hole configurations. We have been concerned in this paper with the falloff behavior of conformal scalar waves in a background geometry which is an asymptotically anti–de Sitter geometry. We found that the waves in uncharged static and spinning 3D black hole backgrounds die out at an exponential rate. This conclusion is supported by both analytical and numerical computations. For conformal scalar waves in a Schwarzschild–anti-de Sitter background our numerical analysis demonstrates that the falloff pattern over short time scales obeys (after some ringing) a power-law falloff. However, over longer time scales the outgoing wave returns from spatial infinity. The falloff of the peak amplitude in this case is neither inverse power nor exponential. However, there is a very weak exponential decrease in the maximal peak amplitude. This decay pattern is so complicated that further investigation will be needed to more precisely determine its dependence on t.

Previous investigations of mass inflation in a charged spinless 3D black hole [13] and an uncharged spinning 3D black hole [16] assumed a power-law falloff rate for the scalar wave. Under such assumptions these investigations demonstrated that mass inflation occurred in the corresponding geometries. We have shown here that the assumption of power-law falloff in the uncharged static and spinning 3D black hole background is not valid and must be replaced by an exponential falloff.

TABLE I. Exponential falloff rate α which is found by graphical method is always less than the surface gravity κ in rotating 3D black holes.

$\lvert\Lambda\rvert$	M	J	$\lvert\Lambda\rvert J^2/M^2$	$\alpha/2$	κ
0.1	0.5	0.001	4×10^{-7}	0.3171	707.107
0.1	0.1	0.001	10^{-5}	0.1413	63.2452
1.0	1.0	0.01	10^{-4}	1.417	199.987
0.1	0.01	0.001	10^{-3}	0.04422	1.99875
0.5	0.01	0.001	5×10^{-3}	0.09852	1.99374
0.1	0.005	0.01	0.4	0.02034	0.0515936
0.2	0.005	0.01	0.8	0.01541	0.0268999

For a rotating 3D black hole we have shown that a ϕ-independent scalar field also has late time exponential decay. In this particular setup, one can recalculate the mass inflation rate using the correct late time falloff rate. It is not difficult to show that the new inflation rate reads $m(v) \propto \exp[(\kappa-\alpha)v]$, where κ is the surface gravity at the Cauchy horizon of the black hole. The parameter α comes from the exponential falloff rate for the scalar wave which reads $\exp(-\alpha t/2)$. For example, when $\Lambda=-0.1$, $M=0.01$, and $J=0.001$, the surface gravity at the Cauchy horizon is 1.999 but the parameter α is only 0.08 according to Fig. 14. Table I shows some other values of α and κ in the rotating 3D black hole backgrounds. For $|\Lambda|J^2/M^2<0.64$ we find that the surface gravity κ is always greater than the exponential falloff rate α. Therefore the attenuation from the falloff effect does not halt mass inflation and the basic conclusions in [16] remain unchanged. Rather the mass inflation rate is slowed down relative to spacetimes with power-law falloff. However, for $|\Lambda|J^2/M^2>0.64$ we find that $\alpha>\kappa$ and mass inflation is attenuated. This case is currently under investigation.

In the nonspinning case in $(2+1)$ dimensions, we find that α is independent of the angular harmonic parameter l. Recall that in Eqs. (87) and (91), l determines the frequency of the quasinormal ringing. The decay rate is governed by λ which is a function of black hole parameters, namely, Λ and M. This leads to a qualitative distinction between the mass inflation mechanism in the (static) $(2+1)$- and $(3+1)$-dimensional spacetimes. In a Schwarzschild background, the falloff rate is $1/t^{2l+3}$ [9] which implies larger the moment l, faster the falloff. This yields a mass inflation rate $\sim\exp(\kappa v)/v^{2(2l+3)}$ [7]; the exponential growth always surpasses the falloff effect for arbitrarily large l. For a 3D black hole with an inner horizon we showed that the falloff rate is exponential which is much stronger than the inverse power falloff. However, this exponential decay is independent of the moment l — unlike the Schwarzschild case, increasing the moment does not yield a stronger attenuation of the mass function.

ACKNOWLEDGMENTS

This work was supported in part by the Natural Sciences and Engineering Research Council of Canada.

APPENDIX: SOLUTIONS IN ASYMPTOTICALLY FLAT $(D+1)$-DIMENSIONAL BACKGROUND

Given the lapse function (23) in $(D+1)$-dimensional spacetime, the time-independent solution of $\mathcal{L}[\psi(r)]=0$ is given by Eq. (25). The coefficients $a_j(r)$ and $c_j(r)$ can be generated by the next two equations:

$$a_{j+1}(r)=m(\ln|r|)^{\beta}a_j(r)-\frac{m[\xi(D-2-\alpha)(D-1-\alpha)+l(l+D-2-\alpha)]}{2\gamma+1}W(1+(j+1)\alpha,(\ln|r|)^{\beta}a_j(r))$$
$$+\frac{m[\xi(D-2-\alpha)(D-1-\alpha)+(l+\alpha)(l+D-2)]}{2\gamma+1}W(2\gamma+2+(j+1)\alpha,(\ln|r|)^{\beta}a_j(r))$$
$$-\frac{m\beta[\xi(2D-3-2\alpha)+l]}{2\gamma+1}W(1+(j+1)\alpha,(\ln|r|)^{\beta-1}a_j(r))+\frac{m\beta[\xi(2D-3-2\alpha)-l-D+2]}{2\gamma+1}$$
$$\times W(2\gamma+2+(j+1)\alpha,(\ln|r|)^{\beta-1}a_j(r))-\frac{m\beta(\beta-1)\xi}{2\gamma+1}W(1+(j+1)\alpha,(\ln|r|)^{\beta-2}a_j(r))$$
$$+\frac{m\beta(\beta-1)\xi}{2\gamma+1}W(2\gamma+2+(j+1)\alpha,(\ln|r|)^{\beta-2}a_j(r)), \tag{A1}$$

$$c_{j+1}(r)=m(\ln|r|)^{\beta}c_j(r)+\frac{m[\xi(D-2-\alpha)(D-1-\alpha)+(l+\alpha)(l+D-2)]}{2\gamma+1}W(1+(j+1)\alpha,(\ln|r|)^{\beta}c_j(r))$$
$$-\frac{m[\xi(D-2-\alpha)(D-1-\alpha)+l(l+D-2-\alpha)]}{2\gamma+1}W(-2\gamma+(j+1)\alpha,(\ln|r|)^{\beta}c_j(r))$$
$$+\frac{m\beta[\xi(2D-3-2\alpha)-l-D+2]}{2\gamma+1}W(1+(j+1)\alpha,(\ln|r|)^{\beta-1}c_j(r))-\frac{m\beta[\xi(2D-3-2\alpha)+l]}{2\gamma+1}$$
$$\times W(-2\gamma+(j+1)\alpha,(\ln|r|)^{\beta-1}c_j(r))+\frac{m\beta(\beta-1)\xi}{2\gamma+1}W(1+(j+1)\alpha,(\ln|r|)^{\beta-2}c_j(r))$$
$$-\frac{m\beta(\beta-1)\xi}{2\gamma+1}W(-2\gamma+(j+1)\alpha,(\ln|r|)^{\beta-2}c_j(r)). \tag{A2}$$

The function W used above is defined as

$$W(n,f(r))\equiv\frac{r^n}{r}\int\frac{f(r)}{r^n}dr,$$

where n is a real number and $f(r)$ is an integrable function. We evaluate the integral in W in such a way that the integration constant is always set to zero. This function has a property that if $f(r)$ is a constant and $n\neq 1$, then $W(n,f(r))$ gives a constant. When n is unity but $f(r)$ is still a constant, $W(n,f(r))$ is proportional to $\ln|r/\mathcal{R}|$, where $\mathcal{R}$ is some constant of dimension of length. In the case when $f(r)$ is no longer constant but a polynomial of $\ln|r/\mathcal{R}|$, the function W gives another polynomial of $\ln|r/\mathcal{R}|$. The index j in the two equations runs from zero to infinity and the starting coefficients $a_0(r)$ and $c_0(r)$ are two arbitrary constants. It is obvious that when the background is flat, i.e., $m=0$, all the $a_j(r)$ and $c_j(r)$ vanish except a_0 and c_0. If $m\neq 0$, these coefficients are polynomials in $\ln|r/\mathcal{R}|$.

For the equation $\mathcal{L}[C_{i+1}(r)]=2dC_i(r)/dr$ with $\mathcal{L}[C_0(r)]=0$, the solution of $C_i(r)$ is given by

$$C_i(r)=r^{\gamma+1+i}\sum_{j=0}^{\infty}\frac{c_j^i(r)}{r^{j\alpha}}.$$

Each coefficient $c_j^i(r)$ can be calculated by the next two equations:

$$c_0^i(r)=c_0^i=\frac{2^i(2\gamma+1)!(\gamma+i)!}{\gamma!(i)!(2\gamma+1+i)!}c_0,$$

$$c_{j+1}^{i+1}(r)=m(\ln|r|)^{\beta}c_j^{i+1}(r)+\frac{2}{2\gamma+1}[\gamma W(-i+(j+1)\alpha,c_{j+1}^i(r))+(\gamma+1)W(-2\gamma-1-i+(j+1)\alpha,c_{j+1}^i(r))]$$
$$+\frac{m[\xi(D-2-\alpha)(D-1-\alpha)+(l+\alpha)(l+D-2)]}{2\gamma+1}W(-i+(j+1)\alpha,(\ln|r|)^{\beta}c_j^{i+1}(r))$$
$$-\frac{m[\xi(D-2-\alpha)(D-1-\alpha)+l(l+D-2-\alpha)]}{2\gamma+1}W(-2\gamma-1-i+(j+1)\alpha,(\ln|r|)^{\beta}c_j^{i+1}(r))$$

$$+\frac{m\beta[\xi(2D-3-2\alpha)-l-D+2]}{2\gamma+1}W(-i+(j+1)\alpha,(\ln|r|)^{\beta-1}c_j^{i+1}(r))-\frac{m\beta[\xi(2D-3-2\alpha)+l]}{2\gamma+1}$$

$$\times W(-2\gamma-1-i+(j+1)\alpha,(\ln|r|)^{\beta-1}c_j^{i+1}(r))+\frac{m\beta(\beta-1)\xi}{2\gamma+1}W(-i+(j+1)\alpha,(\ln|r|)^{\beta-2}c_j^{i+1}(r))$$

$$-\frac{m\beta(\beta-1)\xi}{2\gamma+1}W(-2\gamma-1-i+(j+1)\alpha,(\ln|r|)^{\beta-2}c_j^{i+1}(r)).$$

[1] S. W. Hawking and G. F. R. Ellis, *The Large Scale Structure of Space-time* (Cambridge University Press, Cambridge, England, 1973).
[2] B. Carter, Phys. Rev. **174**, 1559 (1968).
[3] R. Penrose, in *Battle Rencontres*, edited by C. M. de Witt and J. A. Wheeler (Benjamin, New York, 1968).
[4] M. Simpson and R. Penrose, Int. J. Theor. Phys. **7**, 183 (1973).
[5] S. Chandrasekhar and J. B. Hartle, Proc. R. Soc. London **A384**, 301 (1982).
[6] W. A. Hiscock, Phys. Lett. **83A**, 110 (1981).
[7] E. Poisson and W. Israel, Phys. Lett. B **233**, 74 (1989); E. Poisson and W. Israel, Phys. Rev. D **41**, 1796 (1990).
[8] A. Ori, Phys. Rev. Lett. **67**, 789 (1991).
[9] R. H. Price, Phys. Rev. D **5**, 2419 (1972).
[10] A. Ori, Phys. Rev. Lett. **68**, 2117 (1992).
[11] S. Droz, Phys. Lett. A **191**, 211 (1994).
[12] J. S. F. Chan and R. B. Mann, Class. Quantum Grav. **12**, 351 (1995); Phys. Rev. D **51**, 5428 (1995).
[13] V. Husain, Phys. Rev. D **50**, R2361 (1994).
[14] R. G. Cai and D. F. Zhao, Phys. Lett. A **208**, 281 (1995).
[15] A. Bonanno, Phys. Rev. D **53**, 7373 (1996).
[16] J. S. F. Chan, K. C. K. Chan, R. B. Mann, Phys. Rev. D **54**, 1535 (1996).
[17] F. Mellor and I. Moss, Phys. Rev. D **41**, 403 (1990).
[18] E. S. C. Ching, P. T. Leung, W. M. Suen, and K. Young, Phys. Rev. D **52**, 2118 (1995).
[19] M. Banados, C. Teitelboim, and J. Zanelli, Phys. Rev. Lett. **69**, 1849 (1992); M. Banados, M. Henneaux, C. Teitelboim, and J. Zanelli, Phys. Rev. D **48**, 1506 (1993).
[20] F. J. Zerilli, Phys. Rev. D **2**, 2141 (1970).
[21] G. Lifschytz and M. Ortiz, Phys. Rev. D **49**, 1929 (1994); S. J. Avis, C. J. Isham, and D. Storey, *ibid.* **18**, 3565 (1978).
[22] E. S. C. Ching, P. T. Leung, W. M. Suen, and K. Young, Phys. Rev. Lett. **74**, 2414 (1995).
[23] C. Gundlach, R. H. Price, and J. Pullin, Phys. Rev. D **49**, 883 (1994).
[24] J. D. Brown, J. D. E. Creighton, and R. B. Mann, Phys. Rev. D **50**, 6394 (1994).
[25] I. Ichinose and Y. Satoh, Nucl. Phys. **B447**, 340 (1995).
[26] *Handbook of Mathematical Functions*, edited by M. Abramowitz and I. A. Stegun (Dover, New York, 1970).